THE JOURNAL OF PHYSICAL CHEMISTRY LETTERS
A JOURNAL OF THE AMERICAN CHEMICAL SOCIETY

pubs.acs.org/JPCL

Letter

Laser-Induced Electron Symmetry Restoration in Oriented Molecules Made Simple

ChunMei Liu, Jörn Manz, and Jean Christophe Tremblay*

Cite This: *J. Phys. Chem. Lett.* 2021, 12, 4421−4427

Read Online

ACCESS | Metrics & More | Article Recommendations | Supporting Information

ABSTRACT: Electron symmetry determines many important properties of molecules, from selection rules for photoelectron spectroscopy to symmetry selection rules for chemical reactions. The original electron symmetry is broken if a laser pulse changes the initial state, typically the ground state g, to a superposition of g and an excited state e with different irreducible representations (IRREPs). Quantum dynamics simulations for two examples, the oriented benzene and LiCN molecules, show that the original electron symmetry can be restored by means of a reoptimized π-laser pulse which transfers the component in the excited state e to another state e', or to several others with the same IRREP as the ground state. This method lends itself to much easier experimental applications than all previous ones because it allows the healing of electron symmetry immediately, without any attosecond constraint on the timing of the second pulse.

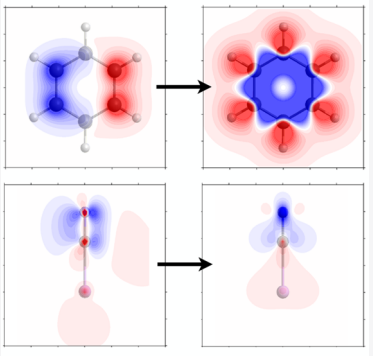

Laser pulses can break electron symmetry in oriented molecules. The phenomenon is obvious from various examples in the literature which document the time evolution of the one-electron density $\rho(t)$ driven by a laser pulse, irrespective of whether the change of electron symmetry was noted explicitly by inspection of $\rho(t)$ (see the first discovery in ref 1) or not.[2−14] The effect can also be rationalized by rigorous point group analyses of the laser-driven quantum dynamics.[15] It opens new opportunities, but it also poses new challenges. On the one hand, it paves the way to laser control of electron symmetry.[15] On the other hand, electron symmetry breaking is undesirable if the original symmetry has favorable properties, e.g., for the selection rules in photoelectron spectroscopy[16] or for electronic symmetry control of chemical reactions.[17] Electron symmetry breaking then calls for prompt symmetry restoration. The literature already has a few suggestions for this purpose, but they all suffer from one big obstacle, namely, the laser pulse for electron symmetry restoration needs perfect timing, with precision of a few attoseconds with respect to the laser pulse which breaks electron symmetry.[18,19] The experimental feasibility has been demonstrated,[18] but it is extremely demanding. This Letter overcomes that obstacle. It presents a method for electron symmetry restoration by means of a laser pulse which can heal broken electron symmetry immediately, without constraint on the timing.

The goal of our approach to electron symmetry restoration is that it must be simple and transferable, must overcome the constraint on attosecond synchronization, and must occur before the onset of asymmetric nuclear motion. It was shown that below ∼10 fs time scale, effects of nuclear motions on electron symmetry are negligible.[20,21] Accordingly, our model considers the nuclear scaffold as rigid. It remains oriented with respect to laboratory fixed coordinates $\{x, y, z\}$, with its center of mass at the origin, and with conservation of nuclear symmetry G.[15,22] Likewise, the electronic ground (g) and excited states (e) transform according to the corresponding irreducible representations (IRREPs) Γ_g and Γ_e of G; in Dirac notation, they are written as $|1\Gamma_g\rangle$ and $|n\Gamma_e\rangle$, respectively, where n denotes the energetic order.

Our scenario assumes that the molecule is initially in the electronic ground state $|1\Gamma_g\rangle$. Electron symmetry is broken by a laser pulse which creates a superposition of $|1\Gamma_g\rangle$ and an excited state $|n\Gamma_e\rangle$ with different IRREP $\Gamma_g \neq \Gamma_e$. The original electron symmetry G is then broken to a subgroup S of G.[15] The concept is to restore electron symmetry S → G by means of a reoptimized π-laser pulse which transfers the component in the excited state $|n\Gamma_e\rangle$ into one or more excited states $|n'\Gamma_{e'}\rangle$ with IRREP $\Gamma_{e'} = \Gamma_g$. This approach will be demonstrated by quantum dynamics simulations for two examples, electron symmetry restoration S → G = C_{2v} → D_{6h} in oriented benzene (after symmetry breaking G → S = D_{6h} → C_{2v}) and electron symmetry restoration C_s → $C_{\infty v}$ in oriented LiCN (after symmetry breaking $C_{\infty v}$ → C_s).

Received: February 28, 2021
Accepted: April 30, 2021
Published: May 5, 2021

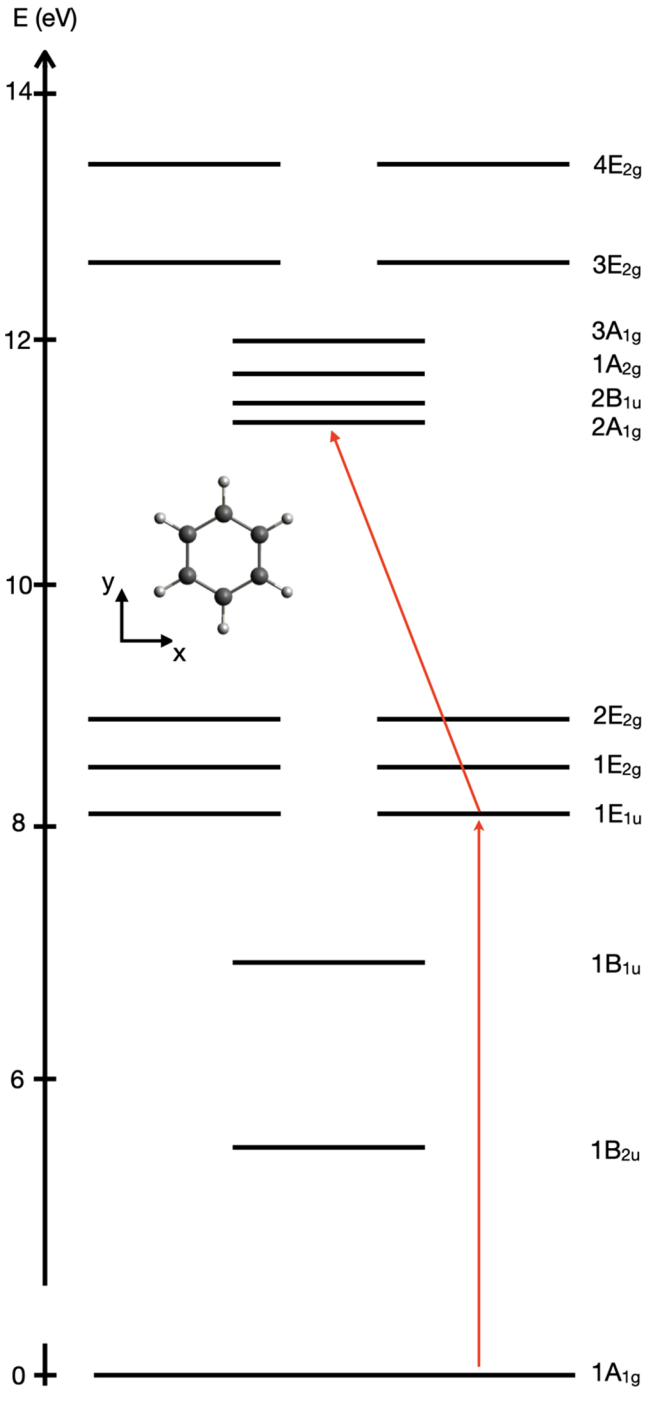

Figure 1. Level diagram of the lowest singlet states of the model benzene, with assignment of the irreducible representations (IRREPs). Nondegenerate and doubly degenerate levels are indicated by single and double horizontal lines, respectively. The rigid nuclear scaffold with point group symmetry G = D_{6h} is oriented in the *xy*-plane, as shown in the inset. The sequential vertical and oblique arrows indicate the target transitions by means of reoptimized $\pi/2$- and π-laser pulses, first from the ground state (here: IRREP A_{1g}) to an excited state with different IRREP (here: E_{1u}), and then to another excited state with the same IRREP as the ground state. The first pulse breaks the symmetry from G to the subgroup S (G → S, with S = C_{2v}) and the second laser pulses restores (S → G) electron symmetry back to G.

The methods are adapted from ref 15 and from the methodological references cited therein. The laser pulses which break and restore electron symmetry are modeled as homogeneous linearly *x*-polarized laser pulses of the form

$$\boldsymbol{\varepsilon}(t) = \begin{cases} \mathbf{e}_x \varepsilon_0 \sin^2[\pi(t - t_i)/T] \sin[\omega(t - t_i - T/2)] & \text{for } t_i \geq t \geq t_i + T \\ \quad \equiv \mathbf{e}_x \varepsilon(t) & \\ 0 & \text{otherwise} \end{cases} \tag{1}$$

where $\mathbf{e}_x$ is the unit vector along *x*, ε_0 the field strength, t_i the initial time, T the pulse duration, ω the carrier frequency, and $\varepsilon(t)$ the scalar field. The corresponding maximum mean intensity at $t = t_i + T/2$ is approximated by $I_m = 0.5 c \epsilon_0 \varepsilon_0^2$ (ϵ_0 and c denote the permittivity of the vacuum and the velocity of light in vacuum, respectively). The laser parameters are specified in the figure captions, with subscripts "b" and "r" for electron symmetry breaking and restoration, respectively. The laser pulse which breaks electron symmetry starts at $t_{ib} = 0$. The laser pulse for electron symmetry restoration is applied immediately after symmetry breaking, $t_{ir} = T_b$, without any constraints of attosecond precision for the timing. In practice, this simplification is the key advantage compared to the methods of refs 18 and 19.

The laser driven electron wave function is expanded in terms of the electronic eigenfunctions

$$|\psi(t)\rangle = \sum_{n\Gamma} c_{n\Gamma}(t) |n\Gamma\rangle \tag{2}$$

The time-dependent coefficients are components of the vector $\mathbf{c}(t)$ which is obtained, in semiclassical dipole approximation, as a solution of the algebraic version of the time-dependent Schrödinger equation (TDSE)

$$i\hbar \frac{\mathrm{d}}{\mathrm{d}t} \mathbf{c}(t) = \mathbf{H}(t)\mathbf{c}(t) \tag{3}$$

with Hamilton matrix elements

$$\mathbf{H}_{n\Gamma,n'\Gamma'}(t) \equiv E_{n\Gamma}\delta_{n\Gamma,n'\Gamma'} - \varepsilon(t)\langle n\Gamma|d_x|n'\Gamma'\rangle \tag{4}$$

where $\delta_{n\Gamma,n'\Gamma'}$ is a Kronecker delta and d_x is the *x*-component of the electronic dipole operator. The energies $E_{n\Gamma}$ and eigenfunctions $|n\Gamma\rangle$ are calculated by means of standard quantum chemistry (see Computational Methods).

The solution of the TDSE (eq 3) allows monitoring of laser driven electron symmetry breaking and restoration in two ways: First, the phenomena are diagnosed by snapshots of the one-electron density $\rho(t)$ calculated from the wave function (eq 2). For better recognition of the laser-induced changes in $\rho(t)$, the figures below show snapshots of the "difference densities" $\rho(t) - \rho_{1\Gamma_g}$. Second, the populations $P_{n\Gamma}(t) = |c_{n\Gamma}(t)|^2$ of states $|n\Gamma\rangle$ (normalized to $\sum_{n\Gamma} P_{n\Gamma}(t) = 1$) provide simple criteria,[15] namely electron symmetry is broken at $t = T_b$ if there are nonzero populations $0 < P_{1\Gamma_g}(t), P_{n\Gamma_e}(t)$ with different IRREPs $\Gamma_e \neq \Gamma_g$. In contrast, electron symmetry is restored at $t = T_b + T_r$ if all populated states have the same IRREP Γ_g, i.e., $P_{n'\Gamma_{e'}}(t) = 0$ for $\Gamma_{e'} \neq \Gamma_g$.

Laser pulses can break electron symmetry in many ways.[15] Here, we employ a reoptimized *x*-polarized $\pi/2$-laser pulse with duration T_b which transfers the initial state $|1\Gamma_g\rangle$ into the superposition of $|1\Gamma_g\rangle$ and target state $|n\Gamma_e\rangle$ with equal populations, $P_{n\Gamma_e}(T_b) = P_{1\Gamma_g}(T_b) = 1/2$. Likewise, electron symmetry is restored by means of a reoptimized *x*-polarized π-laser pulse with duration T_r which is designed to transfer $|n\Gamma_e\rangle$

https://doi.org/10.1021/acs.jpclett.1c00645
J. Phys. Chem. Lett. 2021, 12, 4421−4427

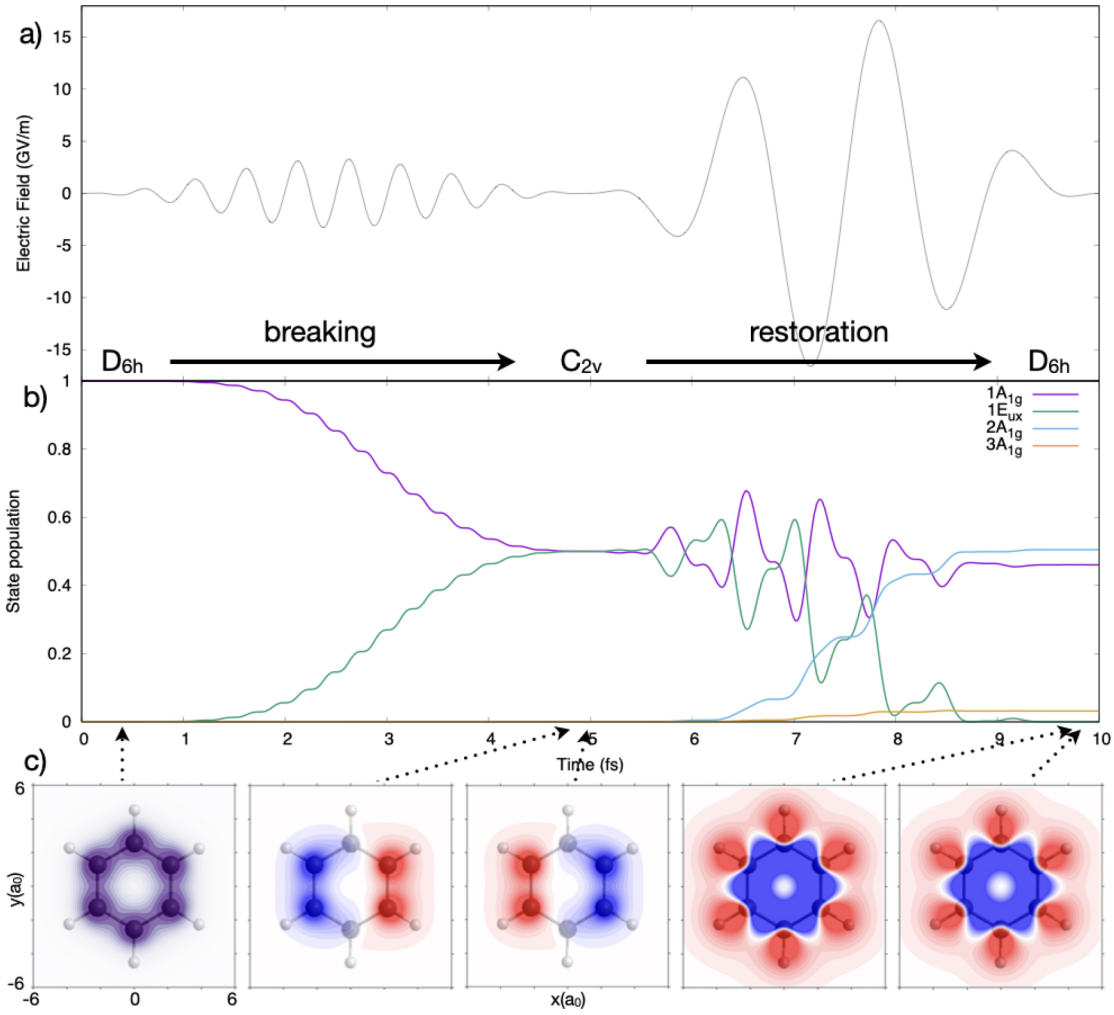

Figure 2. Electron symmetry breaking G → S from point group G to the subgroup S (here: $D_{6h} \rightarrow C_{2v}$) and restoration S → G (here: $C_{2v} \rightarrow D_{6h}$) in the oriented model benzene, by means of two sequential reoptimized $\pi/2$- and π-laser pulses. The corresponding target transitions are indicated by the sequential vertical and oblique arrows in Figure 1. Panels a, b, and c show the electric field, the resulting population dynamics, and snapshots of the original one-electron density and of the difference density driven by the laser pulses, respectively. The fields are specified in eq 1, with parameters $\hbar\omega_b = 8.17$ eV, $\varepsilon_b = 3.31 \times 10^9$ V/m, $I_{mb} = 1.45 \times 10^{12}$ W/cm^2, $t_{ib} = 0$ fs, and $T_b = 5$ fs for symmetry breaking; $\hbar\omega_r = 2.97$ eV, $\varepsilon_r = 1.74 \times 10^{10}$ V/m, $I_{mr} = 4.01 \times 10^{13}$ W/cm^2, $t_{ir} = 5$ fs, and $T_r = 5$ fs for symmetry restoration.

to another excited target state $|n'\Gamma_{e'}\rangle$ with IRREP $\Gamma_{e'} = \Gamma_g$. For reference (see the Supporting Information), in simple three-state $\{|1\Gamma_g\rangle, |n\Gamma_e\rangle, |n'\Gamma_{e'}\rangle\}$ models these transfers are achieved by means of $\pi/2$- and π-pulses (eq 1) with parameters which satisfy the relations $\hbar\omega_b = E_{n\Gamma_e} - E_{1\Gamma_g}$ and $|\langle 1\Gamma_g|d_x|n\Gamma_e\rangle|\varepsilon_{0b}T_b/(2\hbar) = \pi/2$ for symmetry breaking as well as $\hbar\omega_r = |E_{n\Gamma_e} - E_{n'\Gamma_{e'}}|$ and $|\langle n\Gamma_e|d_x|n'\Gamma_{e'}\rangle|\varepsilon_{0r}T_r/(2\hbar) = \pi$ for symmetry restoration, respectively.[15,23] Strictly speaking, these rules call for laser pulses with many cycles, i.e., $T \gg 2\pi/\omega$. The present multistate models for few-cycle laser pulses require slight reoptimizations of these parameters.[15,24]

Our first example is for electron symmetry breaking $D_{6h} \rightarrow C_{2v}$ and restoration $C_{2v} \rightarrow D_{6h}$ in oriented benzene, based on the model described in refs 1, 15, 18, 19, and 25. Its nuclear scaffold transforms according to G = D_{6h} symmetry, and it is oriented in the laboratory xy-plane as illustrated in Figure 1. Its low-lying singlet energy levels $E_{n\Gamma}$ are also shown, with assignments of their IRREPs. The corresponding eigenstates $|n\Gamma_e\rangle$ are included in the expansion (eq 2). The target transitions induced by the laser pulses for symmetry breaking and restoration are also indicated by vertical and oblique arrows. Specifically, the model benzene is initially in its electronic ground state $|1\Gamma_g\rangle = |1A_{1g}\rangle \equiv |1^1A_{1g}\rangle$ (multiplicity is dropped hereafter to simplify notation) with IRREP $\Gamma_g = A_{1g}$.

The initial one-electron density $\rho(t = 0)$ transforms according to the totally symmetric IRREP of G = D_{6h}, as shown in Figure 2c. This symmetry is broken, G → S = $D_{6h} \rightarrow C_{2v}$, by an x-polarized few-cycle reoptimized $\pi/2$-laser pulse with duration $T_b = 5$ fs which creates the superposition of $|1A_{1g}\rangle$ and excited state $|n\Gamma_e\rangle = |1E_{x,1u}\rangle$ transforming to a different IRREP, $\Gamma_e = E_{1u} \neq \Gamma_g = A_{1g}$. The broken symmetry is restored, S → G = $C_{2v} \rightarrow D_{6h}$, by an x-polarized few-cycle pulse with duration $T_r = 5$ fs designed to depopulate excited state $|n\Gamma_e\rangle = |1E_{x,1u}\rangle$ to the target state $|n'\Gamma_{e'}\rangle = |2A_{1g}\rangle$ with IRREP $\Gamma_{e'} = \Gamma_g = A_{1g}$. The field strength $\varepsilon_b(t)$ and $\varepsilon_r(t)$ (eq 1) of the sequential laser pulses for symmetry breaking and restoration are illustrated in Figure 2a (see caption for laser parameters). The resulting population dynamics is shown in Figure 2b; snapshots of the difference densities are in Figure 2c. Two pairs of snapshots taken near $t = T_b = 5$ fs and near $t = T_b + T_r = 10$ fs document periodic and quasi-periodic charge

https://doi.org/10.1021/acs.jpclett.1c00645
J. Phys. Chem. Lett. 2021, 12, 4421−4427

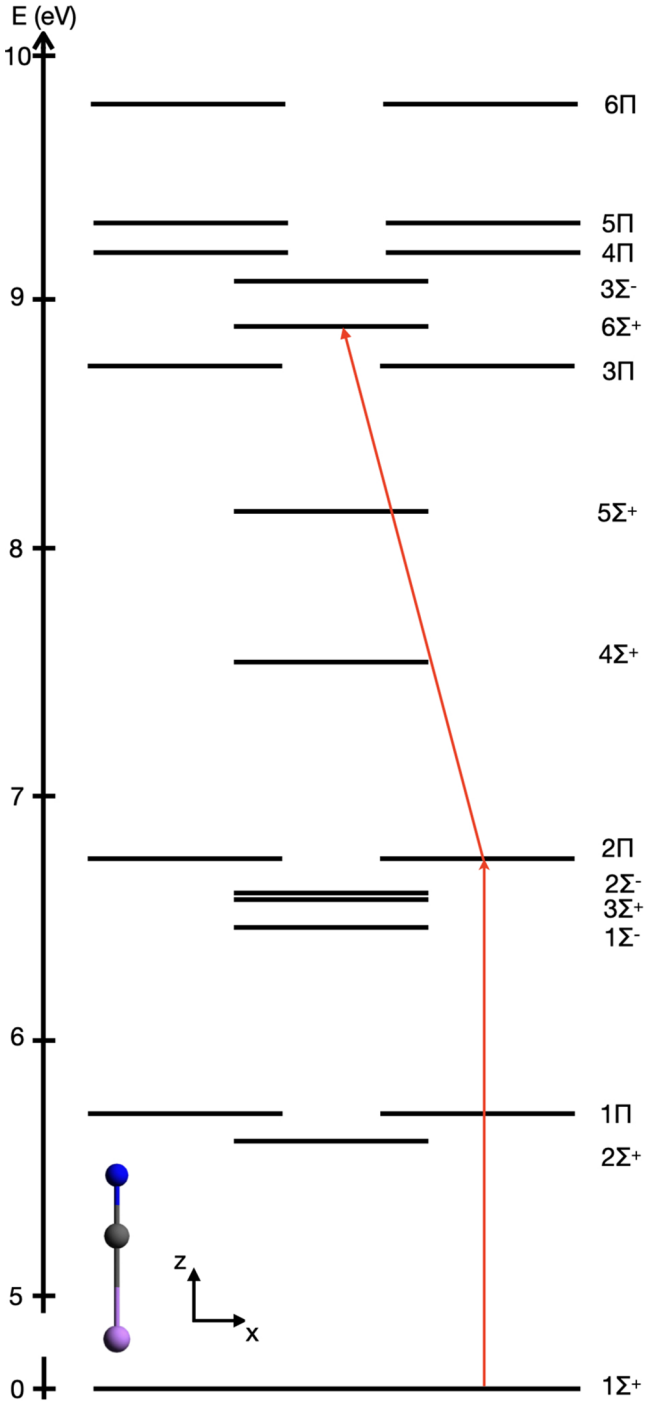

Figure 3. Same as Figure 1, but for electron symmetry breaking and restoration in the oriented LiCN molecule with point group G = $C_{\infty v}$ and subgroup S = C_s. The nondegenerate and doubly degenerate levels have IRREPs Σ^+, Σ^-, and Π, respectively.

migrations with period $T_{1A_{1g}1E_{1u}} = h/(E_{1E_{1u}} - E_{1A_{1g}}) = 506$ as and with dominant period $T_{1A_{1g}2A_{1g}} = h/(E_{2A_{1g}} - E_{1A_{1g}}) = 378$ as at the end of the laser pulses for electron symmetry breaking and restoration, respectively. Obviously, these snapshots manifest laser-driven symmetry breaking $D_{6h} \rightarrow C_{2v}$, immediately followed by successful symmetry restoration $C_{2v} \rightarrow D_{6h}$, respectively. This is confirmed by the criteria for the population dynamics: At $t = T_b = 5$ fs, the populations $P_{1\Gamma_g}(T_b) = P_{1A_{1g}}(T_b) = 1/2$ and $P_{n\Gamma_e}(T_b) = P_{1E_{1u}}(T_b) = 1/2$ of states with different IRREPs $\Gamma_g = A_{1g} \neq \Gamma_e = E_{1u}$ diagnose electron symmetry breaking by the first laser pulse. In contrast, at $t = T_b + T_r = 10$ fs, electron symmetry restoration is diagnosed by exclusive populations of states with IRREP $\Gamma_g = A_{1g}$ and the absence of populations of any other states $|n'\Gamma_{e'}\rangle$ with different IRREPs, $P_{n'\Gamma_{e'}}(T_b + T_r) = 0$ for $\Gamma_{e'} \neq A_{1g}$.

Our second example is for electron symmetry breaking G → S = $C_{\infty v} \rightarrow C_s$ and restoration S → G = $C_s \rightarrow C_{\infty v}$ in oriented LiCN. It uses the model of ref 26. Figure 3 illustrates its orientation along the z-axis, with G = $C_{\infty v}$ nuclear symmetry. This symmetry is also imposed on the one-electronic density of the initial electronic ground state $|1\Gamma_g\rangle = |1\Sigma^+\rangle$ (cf. Figure 4c). The electronic energy levels $E_{n\Gamma}$ below ionization threshold are also shown in Figure 3, with assignments of the IRREPs. The corresponding eigenfunctions $|n\Gamma\rangle$ are included in the expansion (eq 2). Figure 3 also has the vertical and oblique arrows for the target transitions for electron symmetry breaking and restoration, analogous to Figure 1 for oriented benzene.

The results for LiCN are documented in Figure 4, entirely analogous to the results for benzene. Clearly, the snapshots of the difference density (Figure 4c) and the populations $P_{1\Sigma^+}(t)$, $P_{2\Pi_x}(t)$, $P_{5\Sigma^+}(t)$, and $P_{6\Sigma^+}(t)$ (Figure 4b) of the ground state $|1\Sigma^+\rangle$ and the first and second excited target states $|n\Gamma_e\rangle = |2\Pi_x\rangle$ (with IRREP $\Gamma_e = \Pi \neq \Gamma_g = \Sigma^+$) and $|n'\Gamma_{e'}\rangle = |6\Sigma^+\rangle$ (with IRREP $\Gamma_{e'} = \Sigma^+ = \Gamma_g$) at times (near to) $t = T_b = 7$ fs and $t = T_b + T_r = 15$ fs manifest electron symmetry breaking $C_{\infty v} \rightarrow C_s$ and restoration $C_s \rightarrow C_{\infty v}$ in oriented LiCN. The sum of populations of all totally symmetric states (solid black line in Figure 4b)) also demonstrate complete symmetry restoration.

To conclude, the present method for prompt healing of broken electron symmetry is universal. It can be applied not only to the examples, oriented benzene and LiCN as documented in Figures 1−4, but also to any other oriented molecule with nuclear scaffold symmetry G in the electronic ground state. Favorable properties of the molecules include a semirigid molecular scaffold, such that asymmetric vibrations are not rapidly excited, therefore interfering with symmetry restoration. The universality is due to the fact that if electron symmetry breaking G → S is induced by ultrafast dipole-allowed laser transition from the initial state $|1\Gamma_g\rangle$ to an excited state $|n\Gamma_e\rangle$ with different IRREPs, $\Gamma_e \neq \Gamma_g$, then one can always design a reoptimized ultrafast π-laser pulse for dipole-allowed transfer of the excited state $|n\Gamma_e\rangle$ to another excited state $|n'\Gamma_{e'}\rangle$, or to a set of excited states with the same IRREP as the initial state, $\Gamma_{e'} = \Gamma_g$. The choice of the target state $|n'\Gamma'_e\rangle = |n'\Gamma_g\rangle$ should satisfy two criteria: First, the transition dipole element $\langle n'\Gamma_e|d_x|n'\Gamma_g\rangle$ should be large enough to avoid excessively large intensity of the laser pulse for symmetry restoration. Otherwise, it could induce competing processes such as ionization.[27] Second, the laser pulse for symmetry restoration must not excite any competing states $|n''\Gamma''_e\rangle$ with different IRREP $\Gamma''_e \neq \Gamma_g$. In other words, the spectral width of the pulse must not cover the accessible levels of any of those hypothetical competitors.

As a consequence, the reoptimized π-laser pulse prepares a superposition of eigenstates (eq 2), all with the same IRREP Γ_g. Clearly, this "healed" superposition state has the same IRREP Γ_g, thus restoring the original symmetry G.[15] The key advantage of this approach to electron symmetry restoration, compared to all previous ones,[18,19] is that reoptimized π-laser

https://doi.org/10.1021/acs.jpclett.1c00645
J. Phys. Chem. Lett. 2021, 12, 4421−4427

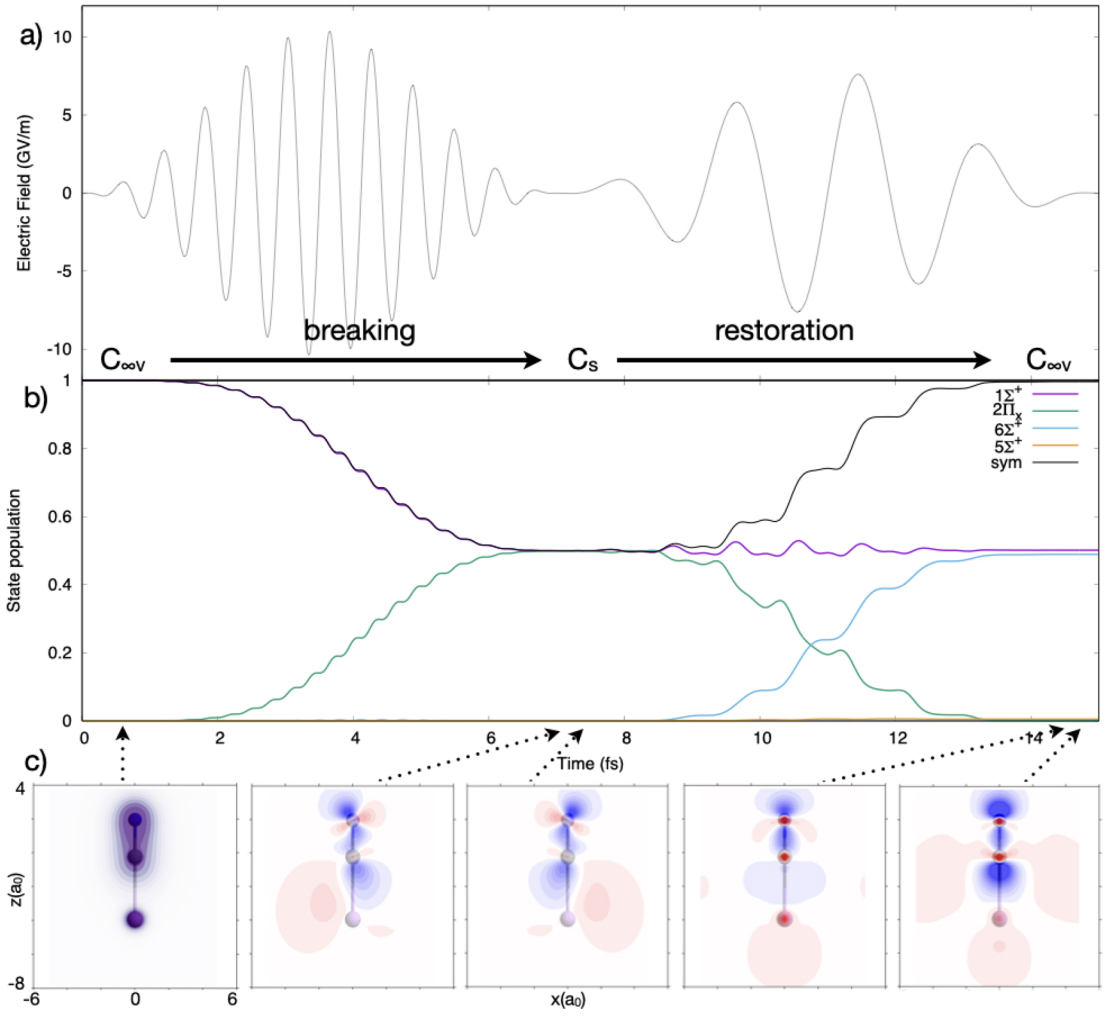

Figure 4. Same as Figure 2, but for the oriented model LiCN with point group G = $C_{\infty v}$ and subgroup S = C_s. The parameters of the laser fields are $\hbar\omega_b$ = 6.73 eV, $\varepsilon_b = 1.04 \times 10^{10}$ V/m, $I_{mb} = 1.44 \times 10^{13}$ W/cm^2, t_{ib} = 0 fs, and T_b = 7 fs for symmetry breaking; $\hbar\omega_r$ = 2.25 eV, $\varepsilon_r = 7.86 \times 10^9$ V/m, $I_{mr} = 8.20 \times 10^{12}$ W/cm^2, t_{ir} = 7 fs, and T_r = 8 fs for symmetry restoration.

pulses aim at population transfer—they can be fired at any time. In contrast, the previous methods employ laser pulses for driving wave functions to selective target states with the desired symmetry; this task calls for control of not only populations but also the phases, implying synchronization with attosecond accuracy. The present method overcomes this obstacle by means of two well-established techniques of coherent control:[23,24,28−30] π-laser pulses and reoptimization. This allows much easier experimental applications than all previous approaches.[18,19] The success profits from the symmetry selection rule for the π-pulse[15] which yields perfect restoration of electron symmetry (see the Supporting Information), calling for just tiny reoptimization of the laser parameters to reach the top of the landscape of optimal control.[31,32] Concepts of experimental techniques for ultrafast monitoring electron symmetry breaking and restoration are in refs 33−37.

As an outlook and working hypothesis, the present approach to laser-induced electron symmetry restoration should stimulate the development of analogous laser-induced nuclear symmetry restoration. Of course, the frequency and time domains will be different, but the roadmap to symmetry restoration should be equivalent. As an example, let us consider the present oriented model benzene. An IR laser pulse might generate the superposition of the vibrational ground and excited states $|1a_{1g}\rangle$ and $|1e_{x,1u}\rangle$,[38] analogous to the UV pulse which generates the superposition of electronic states $|1A_{1g}\rangle$ and $|1E_{x,1u}\rangle$. Both cases imply $D_{6h} \rightarrow C_{2v}$ symmetry breaking, either for the coherent vibrations of the nuclear densities[39−41] or for charge migration of the electronic density (cf. Figure 2). Nuclear symmetry could be restored ($C_{2v} \rightarrow D_{6h}$) by an IR pulse which transfers the vibrational state $|1e_{x,1u}\rangle$ to an excited state $|na_{1g}\rangle$, analogous to electronic symmetry restoration by population transfer from $|1E_{x,1u}\rangle$ to the excited state $|nA_{1g}\rangle$. As a byproduct, the nuclear symmetry breaking and restoration would be accompanied by coherent electronic symmetry breaking and restoration. This example is encouraging for extensions of the present approach to laser-induced coherent electronic and nuclear symmetry restoration. For the time being we recommend, however, to keep the present limit of about 10−15 fs for pure electron symmetry restoration.

■ COMPUTATIONAL METHODS

The electronic structure of benzene is calculated using state-averaged CASSCF(6,6) with an aug-cc-pVTZ basis[42] as implemented in MOLPRO.[43] The energies of the 15 lowest excited states are corrected by multireference configuration interaction with single and double excitations. The electronic

https://doi.org/10.1021/acs.jpclett.1c00645
J. Phys. Chem. Lett. 2021, 12, 4421−4427

structure of LiCN is calculated at the TDDFT/aug-cc-pVTZ[42] level of theory using the CAM-B3LYP functional,[44] as implemented in Gaussian16.[45] The geometries used can be found in the Supporting Information. Electronic densities are generated using ORBKIT,[46−48] integrated over the coordinate perpendicular to the paper plane and plotted using Matplotlib.[49] The transition dipole matrix elements $\langle n\Gamma|d_x|n'\Gamma'\rangle$ are computed from the wave functions using detCI@ORBKIT.[46−48] The TDSE (eq 3) is solved by means of the time-dependent configuration interaction methodology in its reduced density matrix formulation (ρ-TDCI).[50] The system is initialized in the ground state $|1\Gamma_g\rangle$, i.e., $c_{n\Gamma}(t=0) = \delta_{n\Gamma,1\Gamma_g}$. Numerically converged results are obtained by including a sufficiently large number of states in the expansion (eq 2). All nonlinear effects during the laser excitation due to the field−molecule interactions are treated variationally and thus are included to all orders in the ρ-TDCI scheme.

■ ASSOCIATED CONTENT

Supporting Information

The Supporting Information is available free of charge at https://pubs.acs.org/doi/10.1021/acs.jpclett.1c00645.

Nuclear coordinates; reference three-state model for electron symmetry breaking and restoration (PDF)

■ AUTHOR INFORMATION

Corresponding Author

Jean Christophe Tremblay − *Laboratoire de Physique et Chimie Théoriques, CNRS-Université de Lorraine, 57070 Metz, France;* orcid.org/0000-0001-8021-7063; Email: jean-christophe.tremblay@univ-lorraine.fr

Authors

ChunMei Liu − *College of Science, Nanjing University of Posts and Telecommunications, Nanjing 210023, China*

Jörn Manz − *Institut für Chemie und Biochemie, Freie Universität Berlin, 14195 Berlin, Germany; State Key Laboratory of Quantum Optics and Quantum Optics Devices, Institute of Laser Spectroscopy, Shanxi University, Taiyuan 030006, China; Collaborative Innovation Center of Extreme Optics, Shanxi University, Taiyuan 030006, China;* orcid.org/0000-0002-9142-8090

Complete contact information is available at: https://pubs.acs.org/10.1021/acs.jpclett.1c00645

Notes

The authors declare no competing financial interest.

■ ACKNOWLEDGMENTS

We are grateful to Professors Dietrich Haase (FU Berlin) and Misha Yu. Ivanov, Olga Smirnova, Marc V.V. Vrakking (MBI Berlin), and Hans Jakob Wörner (ETH Zürich) for advice during the revision of this Letter and to Professor Beate Paulus (Freie Universität Berlin) for continuous support of our cooperation. This work profits from financial support, in part by the National Key Research and Development Program of China (2017YFA0304203), the Program for Changjiang Scholars and Innovative Research Team (IRT_17R70), the National Natural Science Foundation of China (No. 11904215 and No. 12004193), the 111 project (Grant No. D18001), the Fund for Shanxi 1331 Project Key Subjects Construction, the Hundred Talent Program of Shanxi Province, and NJUPT-SF(Grant No. NY220089).

■ REFERENCES

(1) Ulusoy, I. S.; Nest, M. Correlated Electron Dynamics: How Aromaticity Can Be Controlled. *J. Am. Chem. Soc.* **2011**, *133*, 20230−20236.

(2) Ivanov, M. Y.; Corkum, P. B.; Dietrich, P. Coherent Control and Collapse of Symmetry in a Two-Level System in an Intense Laser Field. *Laser Physics* **1993**, *3*, 375−380.

(3) Chelkowski, S.; Yudin, G.; Bandrauk, A. Observing Electron Motion in Molecules. *J. Phys. B: At., Mol. Opt. Phys.* **2006**, *39*, S409−S417.

(4) Remacle, F.; Kienberger, R.; Krausz, F.; Levine, R. D. On the Feasibility of an Ultrafast Purely Electronic Reorganization in Lithium Hydride. *Chem. Phys.* **2007**, *338*, 342−347.

(5) Smirnova, O.; Mairesse, Y.; Patchkovskii, S.; Dudovich, N.; Villeneuve, D.; Corkum, P.; Ivanov, M. Y. High Harmonic Interferometry of Multi-Electron Dynamics in Molecules. *Nature* **2009**, *460*, 972−977.

(6) Mignolet, B.; Levine, R. D.; Remacle, F. Localized Electron Dynamics in Attosecond-Pulse-Excited Molecular Systems: Probing the Time-Dependent Electron Density by Sudden Photoionization. *Phys. Rev. A: At., Mol., Opt. Phys.* **2012**, *86*, 053429.

(7) Li, H.; Mignolet, B.; Wachter, G.; Skruszewicz, S.; Zherebtsov, S.; Süßmann, F.; Kessel, A.; Trushin, S. A.; Kling, N. G.; Kübel, M.; et al. Coherent Electronic Wave Packet Motion in C_{60} Controlled by the Waveform and Polarization of Few-Cycle Laser Fields. *Phys. Rev. Lett.* **2015**, *114*, 123004.

(8) Bruner, B. D.; Mašín, Z.; Negro, M.; Morales, F.; Brambila, D.; Devetta, M.; Faccialà, D.; Harvey, A. G.; Ivanov, M.; Mairesse, Y.; et al. Multidimensional High Harmonic Spectroscopy of Polyatomic Molecules: Detecting Sub-Cycle Laser-Driven Hole Dynamics upon Ionization in Strong Mid-IR Laser Fields. *Faraday Discuss.* **2016**, *194*, 369−405.

(9) Chandra, S.; Bhattacharya, A. Attochemistry of Ionized Halogen, Chalcogen, Pnicogen, and Tetrel Noncovalent Bonded Clusters. *J. Phys. Chem. A* **2016**, *120*, 10057−10071.

(10) Yuan, K.-J.; Shu, C.-C.; Dong, D.; Bandrauk, A. D. Attosecond Dynamics of Molecular Electronic Ring Currents. *J. Phys. Chem. Lett.* **2017**, *8*, 2229−2235.

(11) Wu, W.-Y.; He, F. Angle-Dependent Electron-Electron Correlation in the Single Ionization of H_2 in Strong Laser Fields. *Sci. Rep.* **2018**, *8*, 14933.

(12) Yuan, K.-J.; Bandrauk, A. D. Time-Resolved Photoelectron Imaging of Molecular Coherent Excitation and Charge Migration by Ultrashort Laser Pulses. *J. Phys. Chem. A* **2018**, *122*, 2241−2249.

(13) He, M.; Li, Y.; Zhou, Y.; Li, M.; Cao, W.; Lu, P. Direct Visualization of Valence Electron Motion using Strong-Field Photoelectron Holography. *Phys. Rev. Lett.* **2018**, *120*, 133204.

(14) Yuan, K.-J.; Bandrauk, A. D. Ultrafast X-ray Photoelectron Imaging of Attosecond Electron Dynamics in Molecular Coherent Excitation. *J. Phys. Chem. A* **2019**, *123*, 1328−1336.

(15) Haase, D.; Hermann, G.; Manz, J.; Pohl, V.; Tremblay, J. C. Electron Symmetry Breaking during Attosecond Charge Migration Induced by Laser Pulses: Point Group Analyses for Quantum Dynamics. *Symmetry* **2021**, *13*, 205.

(16) Quack, M.; Merkt, F. *Handbook of High-Resolution Spectroscopy*; Wiley: Chichester, 2011; Vol. *1*.

(17) Woodward, R. B.; Hoffmann, R. The Conservation of Orbital Symmetry. *Angew. Chem., Int. Ed. Engl.* **1969**, *8*, 781−853.

(18) Liu, C.; Manz, J.; Ohmori, K.; Sommer, C.; Takei, N.; Tremblay, J. C.; Zhang, Y. Attosecond Control of Restoration of Electronic Structure Symmetry. *Phys. Rev. Lett.* **2018**, *121*, 173201.

(19) Liu, C.; Manz, J.; Tremblay, J. C. From Symmetry Breaking via Charge Migration to Symmetry Restoration in Electronic Ground and Excited States: Quantum Control on the Attosecond Time Scale. *Appl. Sci.* **2019**, *9*, 953.

(20) Mineo, H.; Lin, S. H.; Fujimura, Y. Vibrational Effects on UV/Vis Laser-Driven π-Electron Ring Currents in Aromatic Ring Molecules. *Chem. Phys.* **2014**, *442*, 103−110.
(21) Despré, V.; Marciniak, A.; Loriot, V.; Galbraith, M. C. E.; Rouzée, A.; Vrakking, M. J. J.; Lépine, F.; Kuleff, A. I. Attosecond Hole Migration in Benzene Molecules Surviving Nuclear Motion. *J. Phys. Chem. Lett.* **2015**, *6*, 426−431.
(22) Haase, D.; Manz, J.; Tremblay, J. C. Attosecond Charge Migration Can Break Electron Symmetry While Conserving Nuclear Symmetry. *J. Phys. Chem. A* **2020**, *124*, 3329−3334.
(23) Tannor, D. J. *Introduction to Quantum Mechanics: A Time-Dependent Perspective*; University Science Books, 2007.
(24) Barth, I.; Manz, J. Periodic Electron Circulation Induced by Circularly Polarized Laser Pulses: Quantum Model Simulations for Mg Porphyrin. *Angew. Chem., Int. Ed.* **2006**, *45*, 2962−2965.
(25) Jia, D.; Manz, J.; Paulus, B.; Pohl, V.; Tremblay, J. C.; Yang, Y. Quantum Control of Electronic Fluxes during Adiabatic Attosecond Charge Migration in Degenerate Superposition States of Benzene. *Chem. Phys.* **2017**, *482*, 146−159.
(26) Klinkusch, S.; Tremblay, J. C. Resolution-of-Identity Stochastic Time-Dependent Configuration Interaction for Dissipative Electron Dynamics in Strong Fields. *J. Chem. Phys.* **2016**, *144*, 184108.
(27) Yudin, G. L.; Ivanov, M. Y. Nonadiabatic Tunnel Ionization: Looking inside a Laser Cycle. *Phys. Rev. A: At., Mol., Opt. Phys.* **2001**, *64*, 013409.
(28) Rice, S. A.; Zhao, M. *Optical Control of Molecular Dynamics*; John Wiley: New York, United States, 2000.
(29) Shapiro, M.; Brumer, P. *Quantum Control of Molecular Processes*, 2nd ed.; John Wiley & Sons: Weinheim, Germany, 2012.
(30) Brif, C.; Chakrabarti, R.; Rabitz, H. Control of Quantum Phenomena: Past, Present and Future. *New J. Phys.* **2010**, *12*, 075008.
(31) Rabitz, H.; Wu, R.-B.; Ho, T.-S.; Moore Tibbetts, K.; Feng, X. In *Recent Advances in the Theory and Application of Fitness Landscapes*; Richter, H., Engelbrecht, A., Eds.; Springer: Berlin, 2014; pp 33−70.
(32) Russell, B.; Rabitz, H. Common Foundations of Optimal Control Across the Sciences: Evidence of a Free Lunch. *Philos. Trans. R. Soc., A* **2017**, *375*, 20160210.
(33) Yudin, G. L.; Chelkowski, S.; Itatani, J.; Bandrauk, A. B.; Corkum, P. B. Attosecond Photoionization of Coherently Coupled Electronic States. *Phys. Rev. A: At., Mol., Opt. Phys.* **2005**, *72*, 051401.
(34) Baykusheva, D.; Ahsan, M. S.; Lin, N.; Wörner, H. J. Bicircular High-Harmonic Spectroscopy Reveals Dynamical Symmetries of Atoms and Molecules. *Phys. Rev. Lett.* **2016**, *116*, 123001.
(35) Liu, X.; Zhu, X.; Li, L.; Li, Y.; Zhang, Q.; Lan, P.; Lu, P. Selection Rules of High-Order-Harmonic Generation: Symmetries of Molecules and Laser Fields. *Phys. Rev. A: At., Mol., Opt. Phys.* **2016**, *94*, 033410.
(36) Yuan, K.-J.; Bandrauk, A. D. Symmetry in Circularly Polarized Molecular High-Order Harmonic Generation with Intense Bicircular Laser Pulses. *Phys. Rev. A: At., Mol., Opt. Phys.* **2018**, *97*, 023408.
(37) Yuan, K.-J.; Bandrauk, A. D. Probing Attosecond Electron Coherence in Molecular Charge Migration by Ultrafast X-Ray Photoelectron Imaging. *Appl. Sci.* **2019**, *9*, 1941.
(38) Preuss, M.; Bechstedt, F. Vibrational Spectra of Ammonia, Benzene, and Benzene Adsorbed on Si (001) by First Principles Calculations with Periodic Boundary Conditions. *Phys. Rev. B: Condens. Matter Mater. Phys.* **2006**, *73*, 155413.
(39) Schild, A. On the Probability Density of the Nuclei in a Vibrationally Excited Molecule. *Front. Chem.* **2019**, *7*, 424.
(40) Aieta, C.; Micciarelli, M.; Bertaina, G.; Ceotto, M. Anharmonic Quantum Nuclear Densities from Full Dimensional Vibrational Eigenfunctions with Application to Protonated Glycine. *Nat. Commun.* **2020**, *11*, 4348.
(41) Aieta, C.; Bertaina, G.; Micciarelli, M.; Ceotto, M. Representing Molecular Ground and Excited Vibrational Eigenstates with Nuclear Densities Obtained from Semiclassical Initial Value Representation Molecular Dynamics. *J. Chem. Phys.* **2020**, *153*, 214117.
(42) Dunning, T. H., Jr. Gaussian Basis Sets for Use in Correlated Molecular Calculations. I. The Atoms Boron through Neon and Hydrogen. *J. Chem. Phys.* **1989**, *90*, 1007.
(43) Werner, H.-J.; Knowles, P. J.; Knizia, G.; Manby, F. R.; Schütz, M.; Celani, P.; Korona, T.; Lindh, R.; Mitrushenkov, A.; Rauhut, G. *MOLPRO*, ver. 2012.1; A Package of ab initio Programs; 2012 See http://www.molpro.net.
(44) Yanai, T.; Tew, D. P.; Handy, N. C. A New Hybrid Exchange-Correlation Functional using the Coulomb-Attenuating Method (CAM-B3LYP). *Chem. Phys. Lett.* **2004**, *393*, 51−57.
(45) Frisch, M. J.; Trucks, G. W.; Schlegel, H. B.; Scuseria, G. E.; Robb, M. A.; Cheeseman, J. R.; Scalmani, G.; Barone, V.; Petersson, G. A.; Nakatsuji, H. et al. *Gaussian16*, rev. C.01; Gaussian Inc.: Wallingford, CT, 2016.
(46) Hermann, G.; Pohl, V.; Tremblay, J. C.; Paulus, B.; Hege, H.-C.; Schild, A. ORBKIT: A Modular Python Toolbox for Cross-Platform Postprocessing of Quantum Chemical Wavefunction Data. *J. Comput. Chem.* **2016**, *37*, 1511−1520.
(47) Hermann, G.; Pohl, V.; Tremblay, J. C. An Open-Source Framework for Analyzing N-Electron Dynamics. II. Hybrid Density Functional Theory/Configuration Interaction Methodology. *J. Comput. Chem.* **2017**, *38*, 2378−2387.
(48) Pohl, V.; Hermann, G.; Tremblay, J. C. An Open-Source Framework for Analyzing N-Electron Dynamics. I. Multideterminantal Wave Functions. *J. Comput. Chem.* **2017**, *38*, 1515−1527.
(49) Hunter, J. D. Matplotlib: A 2D Graphics Environment. *Comput. Sci. Eng.* **2007**, *9*, 90−95.
(50) Tremblay, J. C.; Klamroth, T.; Saalfrank, P. Time-Dependent Configuration-Interaction Calculations of Laser-Driven Dynamics in Presence of Dissipation. *J. Chem. Phys.* **2008**, *129*, 084302.

https://doi.org/10.1021/acs.jpclett.1c00645
J. Phys. Chem. Lett. 2021, 12, 4421−4427